AIAA-92-2111

AERODYNAMIC SPRING AND DAMPING OF FREE-PITCHING TIPS ON A SEMISPAN WING

Larry A. Young
NASA Ames Research Center
Moffett Field, CA

Daniel M. Martin
Sterling Software
Palo Alto, CA

AIAA Dynamics Specialist Conference
April 16-17, 1992/Dallas, Texas

AERODYNAMIC SPRING AND DAMPING OF FREE-PITCHING TIPS ON A SEMISPAN WING

Larry A. Young*
NASA Ames Research Center
Moffett Field, CA

Daniel M. Martin†
Sterling Software
Palo Alto, CA

Abstract

A test was conducted in the NASA Ames 7- by 10-Foot Wind Tunnel to derive aerodynamic spring and damping estimates for free-pitching tips on a semispan wing. The test model was a rectangular planform semi-span wing with wing tips that had a single rigid-body pitch degree of freedom with respect to the inboard wing. A number of different tip planform geometries were tested, incorporating a range of quarter-chord sweep angles and taper ratios. The wing-tip dynamic response characteristics were measured at several wing angles of attack and tunnel dynamic pressures. The tip oscillations were initiated by releasing the tips from prescribed angles of attack. A new method to isolate Coulomb damping from aerodynamic damping from these tip-motion time histories is developed and applied. Correlations were performed between the experimentally derived wing-tip aerodynamic spring and damping values and predictions from a semiempirical analysis based on steady-state tip aerodynamic loads.

Nomenclature

a	two-dimensional, unsteady, thin-airfoil-theory aerodynamic center offset from pitch axis, referenced to airfoil mid-chord point, m
AR	wing, or tip, aspect ratio
b	airfoil semi-chord length, referenced to airfoil mid-chord point, m
c_0	tip reference chord length (inboard-edge chord), m
C_A	free-pitching wing-tip aerodynamic damping constant, N·m·sec/rad
c_a	nondimensional aerodynamic damping constant
C(k)	Theodorsen lift deficiency function
C_{d_0}	tip zero-lift drag coefficient, drag/(qS_T)
C_L	tip lift coefficient, lift/(qS_T)
C_{L0_T}	tip zero-incidence-angle lift coefficient
$C_{L0_{\alpha W}}$	wing-on-tip interactional aerodynamic coefficient, 1/rad
$C_{L\alpha_T}$	tip lift curve slope as a function of tip incidence angle, 1/rad
C_{m_0}	tip zero-lift pitching-moment coefficient, moment/(qS_Tc_0)
c_{pa}	tip pitch-axis chordwise location (fraction of inboard-edge chord length)
d	decay function, nondimensional
h	tip plunge motion displacement, m
I	tip polar mass moment of inertia, nonaero-dynamic, N·m·sec^2/rad

*Aerospace Engineer, Group Leader.
†Aerospace Engineer, Member AIAA.

I_A	tip virtual polar mass moment of inertia, aerodynamic, N·m·sec^2/rad
K_A	free-pitching wing-tip aerodynamic spring constant, N·m/rad
k_a	nondimensional aerodynamic spring
K_S	mechanical spring rate imposed by the tip pitching mechanism, N·m/rad
K	total spring rate for free-pitching wing tip, $K = K_A + K_S$, N·m/rad
M_A	aerodynamic pitching moment, negative nose-down moment, N·m
M_d	tip Coulomb (friction) damping moment, (opposes tip motion), negative nose-down moment, N·m
M_S	tip mechanical spring moment, negative nose-down moment, N·m
q	free-stream dynamic pressure, kPa
r	effective friction moment arm of the free-pitching tip pitching mechanism, m
S_T	tip planform area, m^2
t	time, sec
U	sectional velocity at tip, V·CosΛ, m/sec
V	free-stream velocity, m/sec
x_{ac}	tip aerodynamic center chordwise location (fraction of inboard-edge chord length)
α_T	tip incidence angle, rad
$\alpha_{T_{QS}}$	quasi-steady tip incidence angle subsequent to a tip transient response, including friction resistance influence, rad
$\alpha_{T_{REST}}$	tip steady-state pitching-moment equilibrium incidence angle, without friction, rad
α_{upwash}	induced upwash tip incidence angle due to interactional aerodynamic influence of the inboard baseline wing, rad
α_W	wing incidence angle, rad
$\Delta\alpha_T$	tip transient-response-peaks incidence angles with respect to the quasi-steady tip incidence angle, rad
$\Delta\theta$	relative angle between wing chord line and tip chord line, measured about the tip pitch axis, rad
ρ	free-stream air density, kg/m^3
μ	friction coefficient for wing-tip pitching mechanism, nondimensional
Λ	tip pitch-axis sweep angle, same as wing quarter-chord sweep, rad
τ	period of free-pitching wing-tip transient response, sec
θ_{PT}	tip pretwist angle, i.e., wind-off incidence angle of the tip without mechanical spring deflection, rad
ω	tip natural frequency, rad/sec
ω_d	tip damped frequency, rad/sec
ζ	tip damping ratio, nondimensional
ζ_a	aerodynamic contribution to tip damping ratio, nondimensional

Introduction

A series of low-speed, small-scale semispan wing tests were conducted in the NASA Ames 7- by 10-Foot Wind Tunnel to study the steady-state interactional aerodynamics of a wing and indexed tips.[1-3] The indexed tip configurations (wing/tip configurations that have fixed, discontinuous steps in incidence angle with respect to the inboard wing) studied in Refs. 1-3 simulated the aerodynamics of free-pitching wing tips in steady-state conditions. These wing/tip configurations were tested in support of research into the free-tip rotor concept,[4] shown in Fig. 1. The free-tip rotor concept was conceived as a means of enhancing rotor performance and reducing rotor vibration through the use of free-pitching rotor tips on otherwise conventional rotor blades. The results of the 1/5-scale rotor test described in Ref. 4 have shown the initial feasibility of the rotor concept. However, the prediction of free-tip rotor performance and blade loads has not yet been addressed. The experimental investigation described in this paper was conducted to gain insight

into the fundamental unsteady aerodynamics of free-pitching tips mounted on fixed semispan wings. Once generalized to rotary-wing applications, the present study could lead to improved analyses for predicting free-tip rotor loads and performance and for guiding the design efforts of a new generation of free-tip rotors.

The flow around a free-pitching tip mounted on a helicopter blade is unsteady, transonic, and three-dimensional. Strong aerodynamic interactions between the rotor blade and the free-pitching tip also occur. In the present study, the incompressible, unsteady aerodynamics of free-pitching wing tips have been approximated by using experimental steady-state lift and pitching-moment coefficients as well as two-dimensional (2D) unsteady aerodynamic theory. The aerodynamic spring and damping constants of the tips were derived by a semiempirical method.

This paper describes the proposed semiempirical prediction method used to estimate the free-pitching wing-tip aerodynamic spring and damping constants. An experimental data reduction methodology used to extract the aerodynamic constants from the free-pitching wing tip's transient response is also discussed. Correlation of the semiempirical predictions with the experimentally derived constants is presented and discussed.

Development of Analysis

Semiempirical Spring and Damping Prediction Methodology

The general motion of a free-pitching wing tip mounted on an elastic wing has two degrees of freedom, α_T and h, and is governed by both steady-state and time-dependent tip moment terms. If the wing is assumed to be rigid, the plunge degree of freedom, h, can be eliminated and only one equation needs to be solved to describe the motion (Eq. (1)). This equation of motion has aerodynamic and mechanical spring terms and assumes that there is no external forcing of the wing/tip dynamic system. Additionally, the equation of motion includes both aerodynamic and Coulomb (due to friction in the tip pitching mechanism) damping. Moment due to the wing's interactional aerodynamic influence on the free-pitching wing tip is included via the α_{upwash} term. This term is the induced tip angle of attack resulting from wing upwash, and it is assumed to be time invariant for the purposes of this study, since this study investigates only tip dynamics where the wing angle of attack is held constant.

$$
\begin{aligned}
&(I+I_A)\cdot\frac{d^2}{dt^2}\left(\alpha_T+\alpha_{upwash}\right)\\
&+C_A\cdot\frac{d}{dt}\left(\alpha_T+\alpha_{upwash}\right)\\
&+\left(K_A+K_S\right)\cdot\left(\alpha_T+\alpha_{upwash}\right)\\
&+M_d\cdot\operatorname{sign}\left(\frac{d\alpha_T}{dt}\right)-K_S\cdot\left(\theta_{PT}+\alpha_W\right)\\
&\qquad\qquad -C_{m_0}qS_Tc_0=0 \qquad (1)
\end{aligned}
$$

The Coulomb damping contribution, M_d, is an unknown quantity and must be empirically estimated.

The steady-state aerodynamic loading for the free-pitching wing tip is characterized by the establishment of a pitching-moment equilibrium between the applied moment from the tip pitching mechanism (resulting from the mechanical spring having an initial pretwist) and a restoring moment due to the tip's aerodynamic pitching moment about the tip's pitch axis. This relationship is derived from Eq. (1) by neglecting the inertial terms, and is, simply,

$$M_S=-M_A$$

where

$$M_S=K_S\cdot\left(\theta_{PT}-\Delta\theta\right)$$

$$
\begin{aligned}
M_A=&\left[\left(C_{L0_T}+C_{L0_{\alpha W}}\alpha_W+C_{L\alpha_T}\alpha_T\right)\right.\\
&\left.\cdot\left(c_{pa}-x_{ac}\right)+C_{m_0}\right]\cdot qS_Tc_0
\end{aligned}
$$

and

$$\Delta\theta=\alpha_T-\alpha_W$$

The tip lift coefficient can be accurately represented by the linear relationship $C_L=C_{L0_T}+C_{L0_{\alpha W}}\alpha_W+C_{L\alpha_T}\alpha_T$. Therefore, the steady-state deflection of a free-pitching wing tip (obtained from moment equilibrium) not subject to external forcing is given by the following expression:

$$\alpha_T = \frac{1}{\left[C_{L\alpha_T}\cdot\left(x_{ac}-c_{pa}\right)\cdot qS_Tc_0 + K_S\right]} \cdot\left[K_S\cdot\left(\theta_{PT}+\alpha_W\right) + \left\{C_{L\alpha_T}\alpha_{upwash}\cdot\left(x_{ac}-c_{pa}\right) - C_{m_0}\right\}\cdot qS_Tc_0\right] \quad (2)$$

where

$$\alpha_{upwash} = \frac{\left(C_{L0_T} + C_{L0_{\alpha W}}\alpha_W\right)}{C_{L\alpha_T}}$$

Expressions for the aerodynamic moment terms in Eq. (1) can be derived from unsteady thin-airfoil theory. Unsteady thin-airfoil theory (see, for example, Ref. 5) specifies the following relationship for the unsteady, potential-flow, 2D airfoil aerodynamic pitching moment:

$$M_A = b\cdot\left(\frac{1}{2}+a\right)\cdot C(k) \cdot\left\{2\pi\rho Ub\cdot\left[U\alpha + \frac{dh}{dt} + b\cdot\left(\frac{1}{2}-a\right)\cdot\frac{d\alpha}{dt}\right]\right\} + \pi\rho b^3\cdot\left\{a\cdot\frac{d^2h}{dt^2} - \left(\frac{1}{2}-a\right)\cdot U\cdot\frac{d\alpha}{dt} - b\cdot\left(\frac{1}{8}+a^2\right)\cdot\frac{d^2\alpha}{dt^2}\right\}$$

This 2D, unsteady aerodynamic pitching-moment relationship can be transformed to approximate three-dimensional (3D) free-pitching-wing-tip unsteady aerodynamics by multiplying the right-hand side of the above equation by two terms, $C_{L\alpha_T}/2\pi$ and S_T/c_0, and making the three substitutions $b = 1/2\cdot c_0$, $a = -1/2 + 2\cdot(c_{pa} - x_{ac})$, and $\alpha = \alpha_T + \alpha_{upwash}$. Also, the tip zero-lift pitching-moment contribution is added to the equation. The resulting modified aerodynamic pitching-moment equation now accounts for the 3D viscous flow about the wing tip and the interactional aerodynamic influence of the inboard wing (through the use of the empirical coefficients $C_{L\alpha_T}$, x_{ac}, C_{m_o}, and α_{upwash}). Once these parameters are substituted into the above equation, the plunge degree of freedom is eliminated, and allowance is made for sweep angle, the aerodynamic moment can be rewritten as follows:

$$M_A = C_{m_0}qS_Tc_0 - \left\{K_A\cdot\left(\alpha_T+\alpha_{upwash}\right) + C_A\cdot\frac{d}{dt}\left(\alpha_T+\alpha_{upwash}\right) + I_A\cdot\frac{d^2}{dt^2}\left(\alpha_T+\alpha_{upwash}\right)\right\} \quad (3a)$$

where the aerodynamic spring, damping, and virtual moment of inertia are

$$K_A = qc_0S_T\cdot(\cos\Lambda)^2\cdot C(k)\cdot C_{L\alpha_T}\cdot\left(x_{ac}-c_{pa}\right) \quad (3b)$$

$$C_A = \frac{1}{2}\cdot\rho V\cdot\cos\Lambda\cdot c_0^2S_TC_{L\alpha_T} \cdot\left\{C(k)\cdot\left[\frac{1}{2}\cdot\left(x_{ac}-c_{pa}\right) + \left(x_{ac}-c_{pa}\right)^2\right] + \frac{1}{16} + \frac{1}{8}\cdot\left(x_{ac}-c_{pa}\right)\right\} \quad (3c)$$

$$I_A = \frac{1}{8}\rho c_0^3S_TC_{L\alpha_T} \cdot\left[\frac{3}{32} + \frac{1}{16}\cdot\left(x_{ac}-c_{pa}\right) + \frac{1}{8}\cdot\left(x_{ac}-c_{pa}\right)^2\right] \quad (3d)$$

To complete the analysis development, the semi-empirical aerodynamic spring and damping predictions made in this paper make use of an approximate relationship, good for a reduced frequency up to 0.3, for the Theodorsen lift deficiency.[5] This approximation was found in Ref. 5 to agree reasonably well with the exact solution for the Theodorsen lift deficiency function, and is given by

$$C(k) = \frac{1}{1+\frac{\pi}{2}\cdot k} \quad (3e)$$

where the reduced frequency is

$$k = \frac{\omega c_0}{2V\cdot\cos\Lambda} \quad (3f)$$

Semiempirical aerodynamic spring and damping predictions, based on Eqs. (3a)-(3f), are compared to experimentally derived aerodynamic spring and damping estimates. The methodology for making these experimental estimates is developed below.

Experimental Methodology for Spring and Damping Estimates

Two conventional approaches for estimating spring and damping constants from the free-vibration transient-response time histories of a dynamic system are the logarithmic-decrement (one-degree-of-freedom system) and the moving-block (two or more degrees of freedom)[6] methods. Neither method can account for dynamic systems that have combined viscous and Coulomb damping, such as the free-pitching wing tips studied during this test. The Coulomb damping is the unintentional by-product of the tip pitching mechanism's mechanical friction, whereas the viscous damping is the tip aerodynamic damping. An alternative approach has been developed to analyze the single-degree-of-freedom tip pitching motion. The semi-span wing used in this test was extremely stiff, and its bending displacements were so small that in effect the tip motion is entirely accounted for in the pitch degree of freedom alone.

Experimentally deriving accurate estimates of aerodynamic spring and damping constants for free-pitching wing tips is complicated by the need to separate the Coulomb damping (due to mechanical friction from the tip pitching mechanism) from the aerodynamic damping. Furthermore, because of the inability of the analysis to separate the virtual (aerodynamic) component of the mass moment of inertia from the nonaerodynamic component, virtual mass contributions were neglected in the present study.

The nonlinear free-pitching wing-tip equation of motion (with Coulomb friction included) (Eq. (1)), can be replaced by a piecewise linear equation set, as is conventionally done for Coulomb damping analyses:

$$I\cdot\frac{d^2\alpha_T}{dt^2}+C_A\cdot\frac{d\alpha_T}{dt}+(K_A+K_S)\cdot\alpha_T+M_d=0 \qquad \left(\frac{d\alpha_T}{dt}>0\right)$$

$$I\cdot\frac{d^2\alpha_T}{dt^2}+C_A\cdot\frac{d\alpha_T}{dt}+(K_A+K_S)\cdot\alpha_T-M_d=0 \qquad \left(\frac{d\alpha_T}{dt}<0\right)$$

The time-dependent solution of the combined viscous- and Coulomb-damping differential equation set, for any given *n*th half-cycle, valid only for that half-cycle, is written in terms of the *n*-1 peak angular displacement, and is

$$\alpha_T(t)=\alpha_{T_{n-1}}\cdot e^{-\zeta\omega t}\cdot\mathrm{Cos}(\omega_d t)+\frac{M_d}{K}\cdot\frac{\alpha_{T_{n-1}}}{\left|\alpha_{T_{n-1}}\right|}$$

An expression for the *n*th half-cycle peak angular displacement, defined in terms of the initial tip deflection and valid for the total transient response, can be obtained from the time-dependent half-cycle solution written above by piecewise matching of successive half-cycle amplitudes, and is given by

$$\alpha_{T_n}=\left[\alpha_{T_0}d^n-\frac{M_d}{K}\cdot\frac{\alpha_{T_0}}{\left|\alpha_{T_0}\right|}\cdot(1+d)\cdot\frac{\left(1-d^n\right)}{(1-d)}\right]\cdot\mathrm{Cos}(n\pi)$$

where

$$d=e^{-\pi\left(\frac{\zeta}{\sqrt{1-\zeta^2}}\right)}$$

$$K=K_A+K_S$$

and

$$K=(I+I_A)\cdot\omega^2\approx I\omega^2$$

$$\zeta=\frac{C_A}{2(I+I_A)\omega}\approx\frac{C_A}{2I\omega}$$

$$\omega=\frac{\omega_d}{\sqrt{1-\zeta^2}}$$

$$\omega_d=\frac{2\pi}{\tau}$$

An alternative expression for the combined viscous- and Coulomb-damping transient-response-peak angular displacements is

$$\alpha_{T_n}=\left[\alpha_{T_m}d^{n-m}-\frac{M_d}{K}\cdot\frac{\alpha_{T_m}}{\left|\alpha_{T_m}\right|}\cdot(1+d)\cdot\frac{\left(1-d^{n-m}\right)}{(1-d)}\right]\cdot\mathrm{Cos}\left((n-m)\pi\right)$$

Note that α_{T_0}, α_{T_n}, and α_{T_m} are the tip angular displacements for the zeroth, *n*th, and *m*th half-cycle transient response peaks (where 0, *n*, and *m* are in sequential order).

However, for the purposes of this paper, the inverse problem needs to be solved. For a given transient response

set of half-cycle peak-to-peak angular displacements and half-period time data, the values for the parameters M_d, C_A, and K_A need to be found. Note that I and K_S are known, given both analytical results and experimental measurements, and that I_A is negligible compared to I. There are three solutions derived for this inverse problem: two exact solutions and one solution based on least-squares regression of the transient response data. The solution approach chosen for any given set of free-pitching wing-tip data is dependent on how many half-cycle peaks, including the initial tip deflection, are included in the tip transient response. It is, of course, desirable to include as many data points as possible in making the estimates for aerodynamic spring and damping in order to arrive at the most accurate solution. The three possible solutions to the inverse problem are listed below.

For transient responses with only three half-cycle peaks, a quadratic solution for d can be derived:

$$\left(\Delta\alpha_{T_0} - \Delta\alpha_{T_2}\right)\cdot d^2 + \left(\Delta\alpha_{T_0} + \Delta\alpha_{T_1} - \Delta\alpha_{T_2}\right)\cdot d + \Delta\alpha_{T_1} = 0 \qquad (4)$$

where

$$\alpha_{T_{REST}} = \frac{-d}{1+d}\cdot\Delta\alpha_{T_2} + \frac{M_d}{K}\cdot\frac{\Delta\alpha_{T_2}}{\left|\Delta\alpha_{T_2}\right|}$$

The values for M_d/K are derived from the next equation set shown below, which is applicable for both three- and four-point transient-response data sets. Thus, for transient responses that have four half-cycle data points, including the initial displacement,

$$d = \frac{\left(\Delta\alpha_{T_3} - \Delta\alpha_{T_1}\right)}{\left(\Delta\alpha_{T_0} - \Delta\alpha_{T_2}\right)} \qquad (5)$$

where

$$\alpha_{T_{REST}} = \frac{1}{2\cdot\left(\Delta\alpha_{T_2} + \Delta\alpha_{T_1} - \Delta\alpha_{T_3} - \Delta\alpha_{T_0}\right)} \cdot\left[\left(\Delta\alpha_{T_3} + \Delta\alpha_{T_2}\right)\cdot\left(\Delta\alpha_{T_1} + \Delta\alpha_{T_0}\right) - \left(\Delta\alpha_{T_2} + \Delta\alpha_{T_1}\right)^2\right]$$

and

$$\frac{M_d}{K} = \frac{\left[\left(\Delta\alpha_{T_1} - \Delta\alpha_{T_2}\right) + \left(\Delta\alpha_{T_0} - \Delta\alpha_{T_1}\right)\cdot d\right]}{2\cdot\frac{\Delta\alpha_{T_0}}{\left|\Delta\alpha_{T_0}\right|}\cdot(1+d)}$$

Finally, by least-squares regression analysis, the expression to be used for transient responses that have five or more half-cycle peak angular displacements is given by

$$\sum_{i=0}^{N-3}\sum_{j=0}^{i}\left[(i+1-j)\cdot\left(\Delta\alpha_{T_{i+3}} - \Delta\alpha_{T_{i+1}}\right)\cdot\left(\Delta\alpha_{T_{j+2}} - \Delta\alpha_{T_j}\right)\cdot\mathrm{Cos}\left((i+1-j)\pi\right)\cdot d^{i-j}\right] - \sum_{i=0}^{N-3}\sum_{j=0}^{i}\left[(i+1-j)\cdot\left(\Delta\alpha_{T_{j+2}} - \Delta\alpha_{T_j}\right)^2\cdot d^{2\cdot(i-j)+1}\right] = 0 \qquad (6)$$

where

$$\alpha_{T_{REST}} = \frac{1}{2(N-2)(1+d)}\cdot\sum_{i=0}^{N-2}\left[\left(\Delta\alpha_{T_{i+1}} - \Delta\alpha_{T_{i+2}}\right) + \left(\Delta\alpha_{T_i} - \Delta\alpha_{T_{i+1}} - 2\cdot\Delta\alpha_{T_{i+2}}\right)\cdot d\right]$$

The above expression requires use of the bisection root-solving method to solve for d, where the solution limits $0 < d < 1$ are known, as the response must be underdamped. For Eqs. (4)–(6), the following definition is used:

$$\Delta\alpha_{T_i} = \alpha_{T_i} - \alpha_{T_{QS}}$$

Aerodynamic spring and damping can be estimated from d, once it has been calculated. The remaining equations are

$$\zeta = \sqrt{\frac{(\ln(d))^2}{\left(\pi^2 + (\ln(d))^2\right)}} \qquad (7a)$$

$$\tau = \frac{2}{N-1} \cdot \sum_{i=0}^{N-1} (t_{i+1} - t_i) \qquad (7b)$$

Using standard textbook definitions for ω and ω_d, and the approximations noted earlier in the paper for ζ and K, the free-pitching wing tips' aerodynamic spring and damping can be estimated.

Description of Experimental Apparatus

Semispan Wing Description

Figure 2 is a representative sketch of the semispan wing and wing-tip installation. The rectangular planform semispan wing was vertically mounted in the wind tunnel. The wing profile was defined by the V23010 airfoil section. The wing semispan was 1.041 m (excluding the tips) and the chord was 0.2064 m. The aspect ratio based on the semispan, without the tips, was 5.05. The wing outer edge had an adapter/attachment hole at the wing quarter-chord, to accept a mechanism to allow free-pitching motion for the wing tips. An intermediate airfoil section provided extra space to accommodate the pitching mechanism for one of the tips. With the intermediate airfoil section the wing span increased to 1.184 m.

Wing-Tip Descriptions

The free-pitching wing tips studied in this test were members of two classes of general planform geometries: the FT and the RC series. The tip geometric characteristics are listed in Table 1 (refer to Fig. 3 for further clarification). The static aerodynamic loads of these tips were studied as fixed-indexed tips on a semispan wing (see Refs. 1–3). The FT35T3 tip planform is almost identical in geometry to the tip used in the rotor test reported in Ref. 4. The RC tip planform was defined as a new generation of blade tips for a second-generation free-tip rotor model. The RC tip was designed through use of a potential-flow panel method.[7] Testing the RC tip required the use of the above-mentioned wing intermediate airfoil section. The mechanical spring rate for the FT series tips was 0.12 N·m/rad, and for the RC tip it was 0.08 N·m/rad.

Examination of data noted in Refs. 1–3 for fixed-indexed tips leads to the conclusion that a free-pitching wing tip's steady-state lift and moment coefficients can be expressed in the following manner:

$$C_L = C_{L0_T} + C_{L0_{\alpha W}} \alpha_W + C_{L\alpha_T} \alpha_T \qquad (8a)$$

$$C_m = C_{m_0} + C_L \cdot (c_{pa} - x_{ac}) \qquad (8b)$$

Table 1 Tip geometries and mass moments of inertia

Tip	Sweep	Taper	Planform Area (m^2)	Inertia $\left(\frac{N \cdot m \cdot sec^2}{rad}\right)$
FT35T3	35 deg	0.3	0.0531	1.605E-3
FT35T6	35 deg	0.6	0.0583	2.158E-3
FT45T6	45 deg	0.6	0.0583	3.108E-3
FT20T3	20 deg	0.3	0.0531	1.300E-3
RC1008	——	——	0.0372	1.435E-3

Note that the pitch-axis location of the tips are at the tips' inboard-edge quarter chord. The interactional aerodynamic contribution of the semispan wing to tip lift and pitching moment can be satisfactorily expressed by the second term in the C_L equation.

Empirical relationships for fixed-indexed tip lift and pitching moment, which includes the influence of the wing/tip interactional aerodynamics, can be derived using Eq. (8) and multiple-linear-regression analysis of the data in Refs. 1–3. The data from these references are for wing/fixed-tip geometries very similar to those tested for the free-pitching tips (the same hardware, in many instances). These expressions for tip lift and pitching moment will be used to obtain semiempirical predictions of unsteady aerodynamic spring and damping that will then be correlated with experimental estimates. For the tips studied during this test, the empirical coefficients are given in Table 2. The empirical values noted for the tip lift-curve slopes are in reasonable agreement with "slender-body" theory predictions, i.e., $C_{L\alpha_T} \approx \pi \cdot AR/2$.

Table 2 Aerodynamic coefficients for free-pitching wing tips, accounting for interactional aerodynamics (derived from Refs. 1–3)

Tip	x_{ac}	C_{m_0}	C_{L0_T}	$C_{L0_{\alpha W}}$	$C_{L\alpha_T}$
FT35T3	0.371	–0.003	–0.048	1.32	2.41
FT35T6	0.379	–0.011	–0.031	1.15	2.52
FT45T6	0.436	–0.011	–0.048	1.20	2.41
FT20T3	0.306	–0.008	–0.036	1.32	2.58
RC1008	0.476	–0.018	0.033	2.18	2.69

Initiation of Tip Transient Response

The tip transient responses were initiated manually from a preset initial tip angle of attack. A cotter pin was inserted into the baseline semispan wing outer edge to act as a hard stop to resist the tips' nose-down pitching moment as tunnel speed was increased. A cord was attached to the cotter pin. The cord spanned the upper half of the test section and passed through a hole in the tunnel ceiling. The tip was released from its nonequilibrium incidence angle by a test crewmember pulling the cord and popping the pin out of the tip/wing junction. The time histories of damped oscillatory motion were recorded by using a Hall-effect transducer to measure tip angular deflection. Tunnel speed was constrained by the amount of tip/wing response coupling observed at the higher speeds. Test-section flow quality also limited the maximum tunnel velocity.

Results

Figure 4 is a sample time history of the free-pitching tip transient response. Table 3 contains representative tip peak angular displacement data (tip angle of attack in degrees) as derived from the time histories, used to estimate aerodynamic spring and damping.

Table 3 Tip peak angular displacement data ($q = 0.38$ kPa, $\alpha_W = 12$ deg, $\theta_{PT} = 0$ deg)

FT20T3	t	0.000	0.146	∞		
	α_T (deg)	18.50	−9.25	−7.81		
FT35T3	t	0.000	0.132	0.242	0.359	∞
	α_T	18.50	−17.23	−1.96	−7.13	−6.53
FT35T6	t	0.000	0.125	0.234	∞	
	α_T	18.50	−13.48	−2.59	−7.47	
FT45T6	t	0.000	0.117	0.229	0.355	∞
	α_T	18.50	−15.00	0.69	−5.84	−5.46
RC1008	t	0.000	0.086	0.172	0.250	0.327
	α_T	−13.53	0.99	−8.92	−0.58	−6.27
		0.429	0.499	∞		
		−1.85	−5.38	−3.23		

Steady-State Tip Aerodynamic Characteristics

Figure 5 shows the variation of steady-state tip pitching moment with tip angle of attack for various wing angles of attack. In Fig. 5a, the interactional aerodynamic influence of the wing lift (as a function of wing angle of attack) on tip pitching moment is clearly seen in the incremental shift in the pitching-moment curves as the wing angle of attack is increased. Figure 5b shows the relative agreement of the empirical relationship of Eq. (8) and its associated Table 2 constants (based on balance data) with respect to moment trends measured during this test. The tip pitching-moment curves for this test (moment center at the tip inboard-edge quarter chord) were indirectly estimated from measurements of the tip steady-state angular deflections and estimates of the tip mechanical spring rates. Experimental pitching-moment results from this test and estimates from the empirical relationship of Eq. (8) run parallel to each other with an approximate two-deg tip angle-of-attack offset. This offset is probably due to the difficulties during the test in rigorously matching the zero-lift wing angle of attack with that in previous tests.[1–3] Further, the semispan wing effective aspect ratio is slightly different in this test from those in Refs. 1–3, and thus subtly impacts the wing interactional aerodynamic influence on the tips. Still, it is clear that the empirical relationship of Eq. (8) does adequately approximate the aerodynamic pitching-moment relationship of the tip and the tip/wing interaction for the purposes of this investigation.

An alternate approach to understanding the free-pitching wing tip's steady-state behavior is to study the tips' equilibrium angle of attack as a function of tunnel dynamic pressure, as shown in Fig. 6. As the tunnel speed increases, the tip deflects nose down to maintain pitching-moment equilibrium with the tip pitching mechanism's mechanical restoring moment, until an asymptotic equilibrium angle of attack is reached. This asymptotic angle of attack is primarily a function of wing lift (and, therefore, wing angle of attack). Examination of Eq. (2) reveals that this asymptotic tip angle of attack is given by the expression

$$\alpha_T \Rightarrow \alpha_{upwash} - \frac{C_{m_0}}{C_{L\alpha_T}\left(x_{ac} - c_{pa}\right)}$$

Free-Pitching Tip Aerodynamic Spring

Results illustrating the experimental and predicted variation of aerodynamic spring with dynamic pressure will now be discussed. Generally, the experimental data

support the semiempirical predictions in that the tip aerodynamic spring is linear with respect to dynamic pressure. All tip spring and damping estimates in this paper are plotted without regard for the wing-angle-of-attack operating condition. This is because examination of reduced experimental data (not presented here) reveals a lack of any influence of wing angle of attack on the tip aerodynamic spring constants (or aerodynamic damping). This experimental observation agrees with the semiempirical aerodynamic spring and damping theory, as represented by Eqs. (3a)–(3f). Also, although not shown here, the data indicate that pretwist has little influence on the tip aerodynamic spring.

Figure 7 shows the impact of tip shape on the aerodynamic-spring-versus-dynamic-pressure curves. The correlation agreement between the experimental spring estimates and the predictions is fairly good. The predictions are based upon Eqs. (3a)–(3f) which can only be solved through iteration. The tip aerodynamic spring and damping predictions do take into account the lift deficiency resulting from the tip motion. As the measured and predicted reduced frequencies for the free-pitching wing tips are in the range 0.15 to 0.2, the range of lift deficiency function values, C(k), is approximately 0.75 to 0.8. The experimental aerodynamic spring and damping results, on the other hand, are derived from the data analysis methodology summarized in Eqs. (4)–(7). The aerodynamic spring correlation results are mixed—the semiempirical prediction method both under- and overpredicts the aerodynamic spring for the various tips tested. An alternative approach to reviewing the spring constant trend as a function of tip shape (the tip shape primarily affects the tip aerodynamic center, as all tips have approximately the same lift-curve slope (see Table 2)) can be accomplished by defining a nondimensional aerodynamic spring coefficient:

$$k_a \equiv \frac{K_A}{qS_T c_0}$$

This spring-versus-aerodynamic-center trend can be seen in Fig. 8. Note that the predicted trend in Fig. 8 is based upon quasi-steady aerodynamics, i.e., C(k) = 1, unlike the trends predicted in Figs. 7a–7e. Another drawback of the approach taken in Fig. 8 is that it also ignores small differences in the individual tip lift-curve slopes: a mean tip lift-curve slope value is used for the predicted trend. These simplifications made for the predictions probably account for most of the trend differences noted in Fig. 8.

The impact of wing sweep on the tip aerodynamic spring was also studied. Figure 9 is representative of the aerodynamic-spring-versus-tunnel-dynamic-pressure trend for a 45-deg swept-back wing. The 45-deg swept-back wing yields a reduction of 50% in the sectional dynamic pressure; furthermore, the reduced frequency is increased by approximately 40% as a result of the sectional velocity reduction. It was found that both factors result in a substantial tip aerodynamic spring reduction. The semiempirical prediction, though, appears to underpredict the lift deficiency effect. This is perhaps because of the inability of the prediction method to quantify the detrimental effects of tip/wing junction aerodynamic interference on tip lift-curve slope at large wing-sweep angles.

Free-Pitching Tip Aerodynamic Damping

The following discussion presents the experimental and predicted variation of aerodynamic damping with dynamic pressure for the tips used in this study. Again, the damping predictions are based on Eqs. (3a)–(3f), and the experimental damping values are extracted from the tip transient response time histories by means of Eqs. (4)–(7). The experimental data support the semiempirical predictions in that the tip aerodynamic damping is a parabolic function of free-stream dynamic pressure.

Figure 10 shows the impact of tip shape on the aerodynamic damping as a function of free-stream dynamic pressure. Correlation of the experimental damping results with the semiempirical predictions shows a fair agreement for most of the tips. However, there is a considerable amount of scatter in the damping estimates. The accuracy of the aerodynamic damping estimates is inversely proportional to the magnitude of the combined viscous and Coulomb damping (the greater the overall damping, the less accurate the damping estimate). And, though the tip aerodynamic damping is very small, the Coulomb damping is relatively large and thus adversely impacts the accuracy of the aerodynamic damping estimate.

The aerodynamic damping trend as a function of tip shape (the shape primarily governs the tip aerodynamic center, as all the tested tips have approximately the same lift-curve slope) is best represented by defining a nondimensional aerodynamic damping coefficient as follows:

$$c_a \equiv \sqrt{\frac{2}{\rho q}} \cdot \frac{C_A}{S_T c_0^2}$$

Use of this parameter, and subsequent averaging of the results, in effect "smooths out" the scatter observed in Figs. 10a–10d. The variation of this nondimensional

damping coefficient with aerodynamic center location is illustrated in Fig. 11. The drawbacks of this trend curve are the same as those noted for the nondimensional spring coefficient. With the exception of the FT35T6 tip (Fig. 10b), the correlation results are much improved. It is unclear why the FT35T6 results disagree so badly with the predicted trend.

The accuracy problems with the experimental aerodynamic damping estimates are due to hardware implementation difficulties that were not satisfactorily resolved during the test: substantial mechanical friction in the tip pitching mechanism, and a tip angular displacement transducer that was prone to accuracy problems. In particular, the RC1008 tip, highly swept and tapered for the full span of the tip, had an intermediate airfoil section between the wing and tip. This resulted in a pitching mechanism whose output shaft was cantilevered across the adapter section, which resulted in considerable axial and angular free play. This mechanical free play in two directions created significant scatter in the RC1008 tip transient response time histories, thus adversely affecting the estimation of damping coefficients.

Finally, data were acquired and predictions were made for several tips with the semispan wing swept back 45 deg. A sample plot is shown in Fig. 12. Aerodynamic damping is a parabolic function of tunnel dynamic pressure, and is linearly dependent on velocity. Therefore, use of a 45-deg swept-back wing results in a 30% reduction in the sectional velocity; furthermore, the reduced frequency is then increased by approximately 40% as a result of the sectional velocity reduction. The data show that both factors result in a reduction of tip aerodynamic damping (compare with Fig. 10a), though the percent reduction in damping is not as great as that for the spring.

Forced Motion Response of Free-Pitching Tips

The tip forced response, when fully decoupled from the wing dynamics, is defined by the classical transfer function for a single-degree-of-freedom mass, spring, and damper system. The transfer function is dependent only on the tip damping and frequency ratios. The damping ratio is proportional to the following nondimensional coefficient, which contains only the aerodynamic and not the inertia terms of the damping ratio:

$$\zeta_a \equiv \frac{C_A}{\sqrt{\rho S_T c_0^3 K_A}}$$

The variation of this parameter with aerodynamic center location for the tips tested is shown in Fig. 13. For the most part, the tip damping-ratio coefficient is insensitive to the tip aerodynamic center chordwise location, with the exception of tips with $(x_{ac} - c_{pa}) < 0.06$. As the aerodynamic center offset approaches zero, however, the free-pitching tip becomes neutrally stable and the aerodynamic contribution to the damping ratio asymptotically approaches an infinitely large value. The FT20T3 tip had an aerodynamic center offset less than 0.06, and the tip time histories consequently decayed extremely rapidly compared to the other tested tips. This rapid decay resulted in an insufficient number of test points per transient response to estimate damping values for the FT20T3. Conversely, the single-degree-of-freedom forced-response characteristics of tips having aerodynamic center offsets greater than 0.06 will be approximately the same, based on aerodynamic considerations only.

Conclusions

The research findings summarized in this paper not only support investigations into the fundamental unsteady aerodynamics of free-pitching tips, but also support efforts in the preliminary design of a second-generation model of the free-tip rotor. Three major accomplishments are noted. First, the development of an experimental methodology to estimate free-pitching wing-tip unsteady aerodynamic parameters is described. Second, the refinement of a semiempirical prediction method for free-pitching tips is discussed. Finally, the analysis of transient-response time history data using the developed analysis methodologies to obtain free-pitching wing-tip aerodynamic spring and damping constants is presented.

The unsteady aerodynamic parameters were derived by analyzing the tip transient responses from an initial nonequilibrium tip deflection. Analysis of the free-pitching wing-tip transient response data necessitated the development of a technique to extract the tip aerodynamic damping contribution from the total system damping which included the mechanical Coulomb (friction) damping of the pitching mechanism.

The experimentally derived aerodynamic spring and damping constants were correlated with the semiempirical predictions. The correlation results presented in this paper were mixed. Several tips demonstrated very good correlation, whereas others demonstrated poor correlation. It has been concluded that most of the poor correlation results are chiefly due to the mechanical free play and high Coulomb damping levels of the tip pitching mechanism

and are not caused by fundamental disagreements between the predictions and the experimental data.

Despite some disagreements with experimental data, the semiempirical prediction methodology is able to provide reasonable first-order estimates of free-pitching tip aerodynamic spring and damping that is invaluable for the design of free-tip rotors and perhaps will have applications to fixed-wing aircraft. Furthermore, the unsteady aerodynamic information is not only applicable to passive free-pitching tip applications but can provide helpful insights into active-control applications that use complex aerodynamic control surfaces.

References

1. Van Aken, J. M., "An Investigation of Tip Planform Influence on the Aerodynamic Load Characteristics of a Semispan Wing and Wing Tip," Report 5171-1, The University of Kansas Center for Research, Inc., Lawrence, Kansas, Dec. 1985.

2. Van Aken, J. M., "Experimental Investigation of Wing Tip Aerodynamic Loading," Vertical Lift Aircraft Design Conference of the American Helicopter Society, San Francisco, California, Jan. 1990.

3. Martin, D. M. and Young, L. A., "Experimental Study of an Independently Deflected Tip Mounted on a Semispan Wing," NASA TM 102842, Sept. 1991.

4. Stroub, R. H., Young, L. A, Keys, C., and Cawthorne, M., "Free-Tip Rotor Wind Tunnel Test Results," 41st Annual Forum of the American Helicopter Society, Fort Worth, Texas, 1985.

5. Johnson, W., *Helicopter Theory*, Princeton University Press, Princeton, New Jersey, 1980.

6. Bousman, W. G. and Winkler, D. J., "Application of the Moving-Block Analysis," Paper CP-81-0653, AIAA/ ASME 22nd Structures, Structural Dynamics and Materials Conference, Atlanta, Georgia, 1981.

7. Martin, D. M. and Stroub, R.H., "VSAERO Analysis of Structurally Decoupled Planforms for the Free-Tip Rotor," AIAA Paper 87-2416, Fifth Applied Aerodynamics Conference, Monterey, California, Aug. 1987.

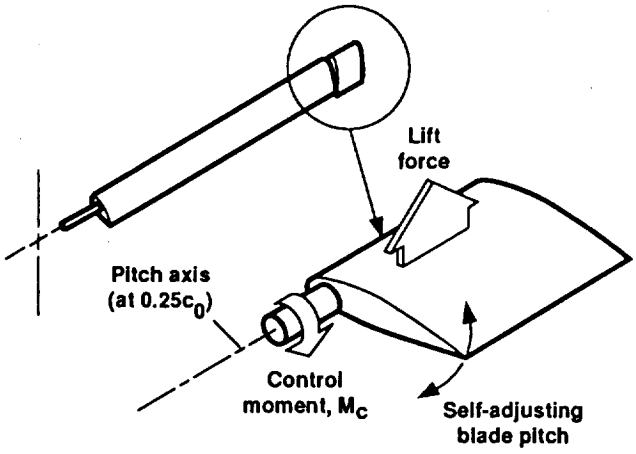

Fig. 1 Free-tip rotor configuration.

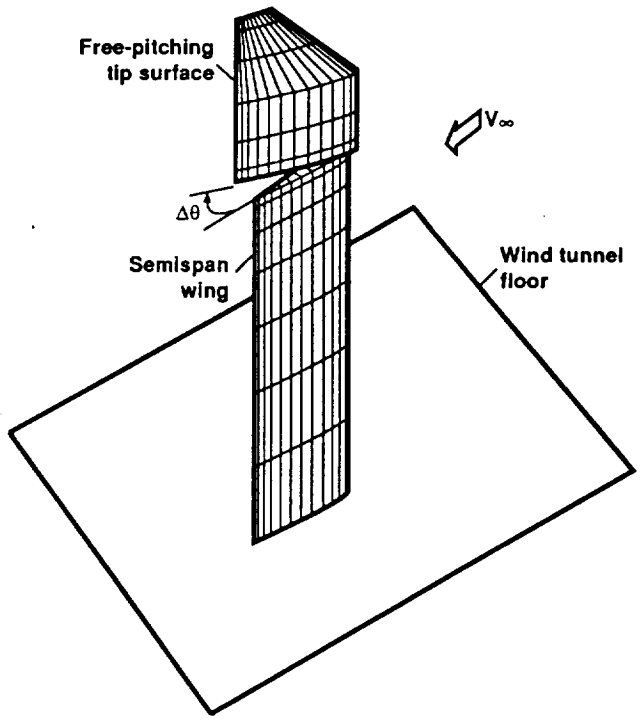

Fig. 2 Wind tunnel installation.

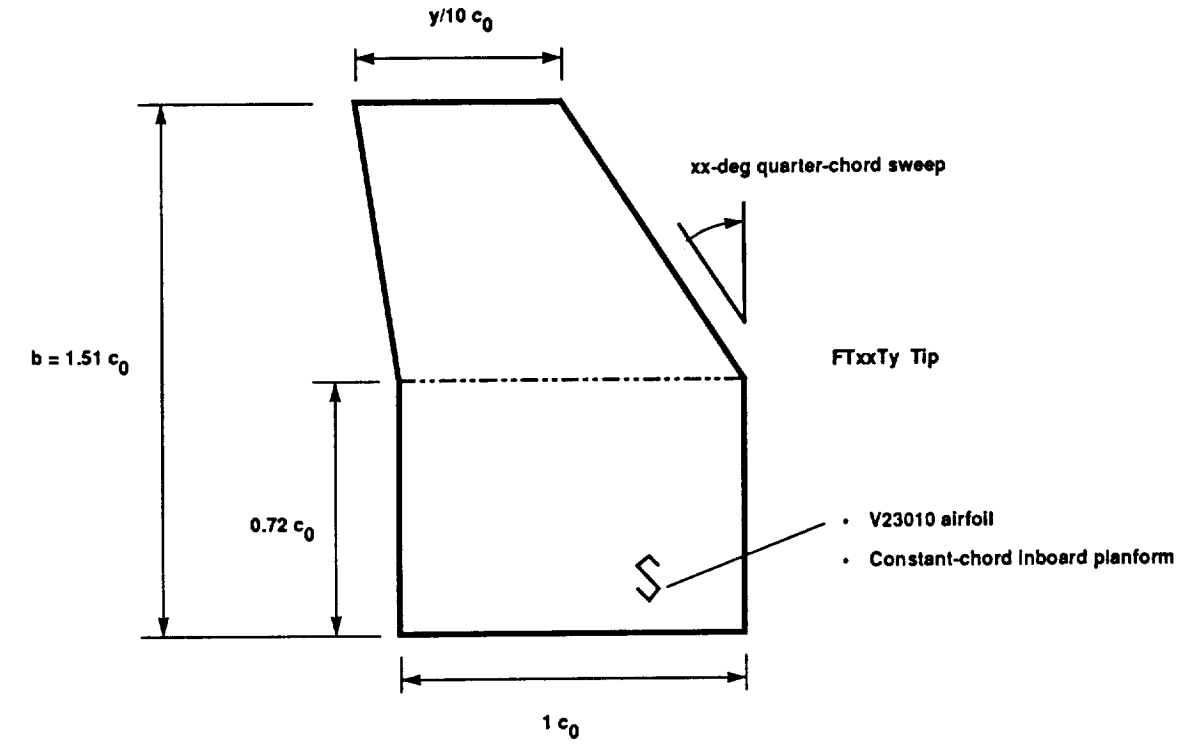

(a)

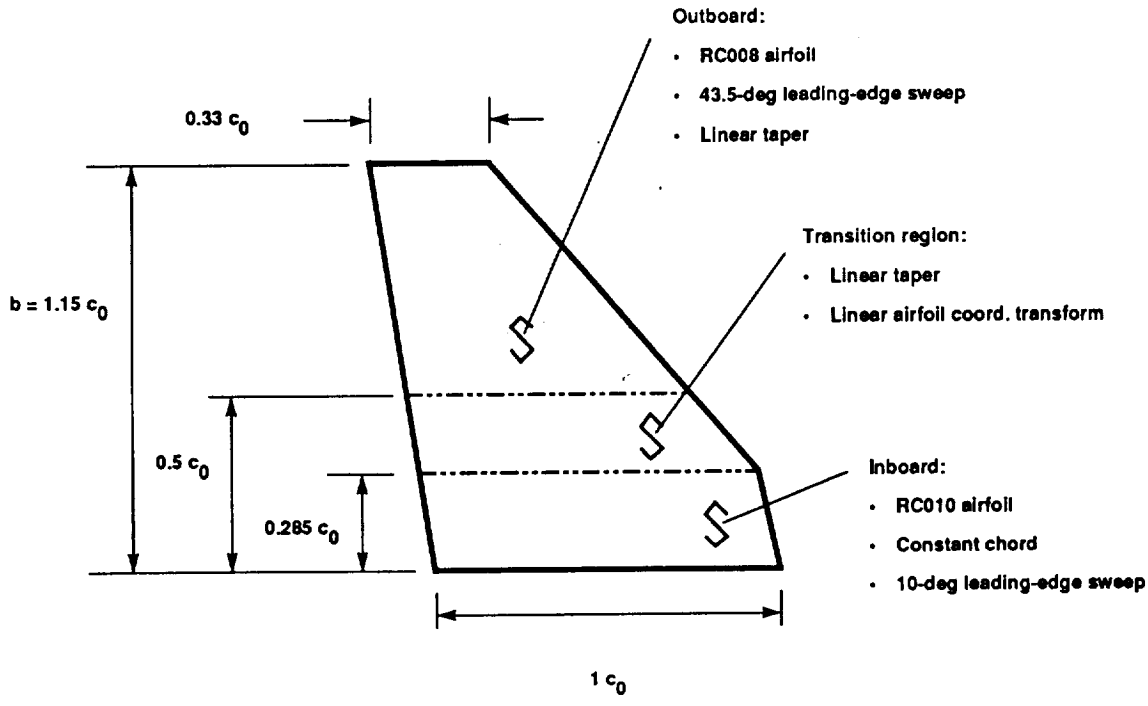

(b)

Fig. 3 Tip planform. a) FT-series tips, b) RC tip.

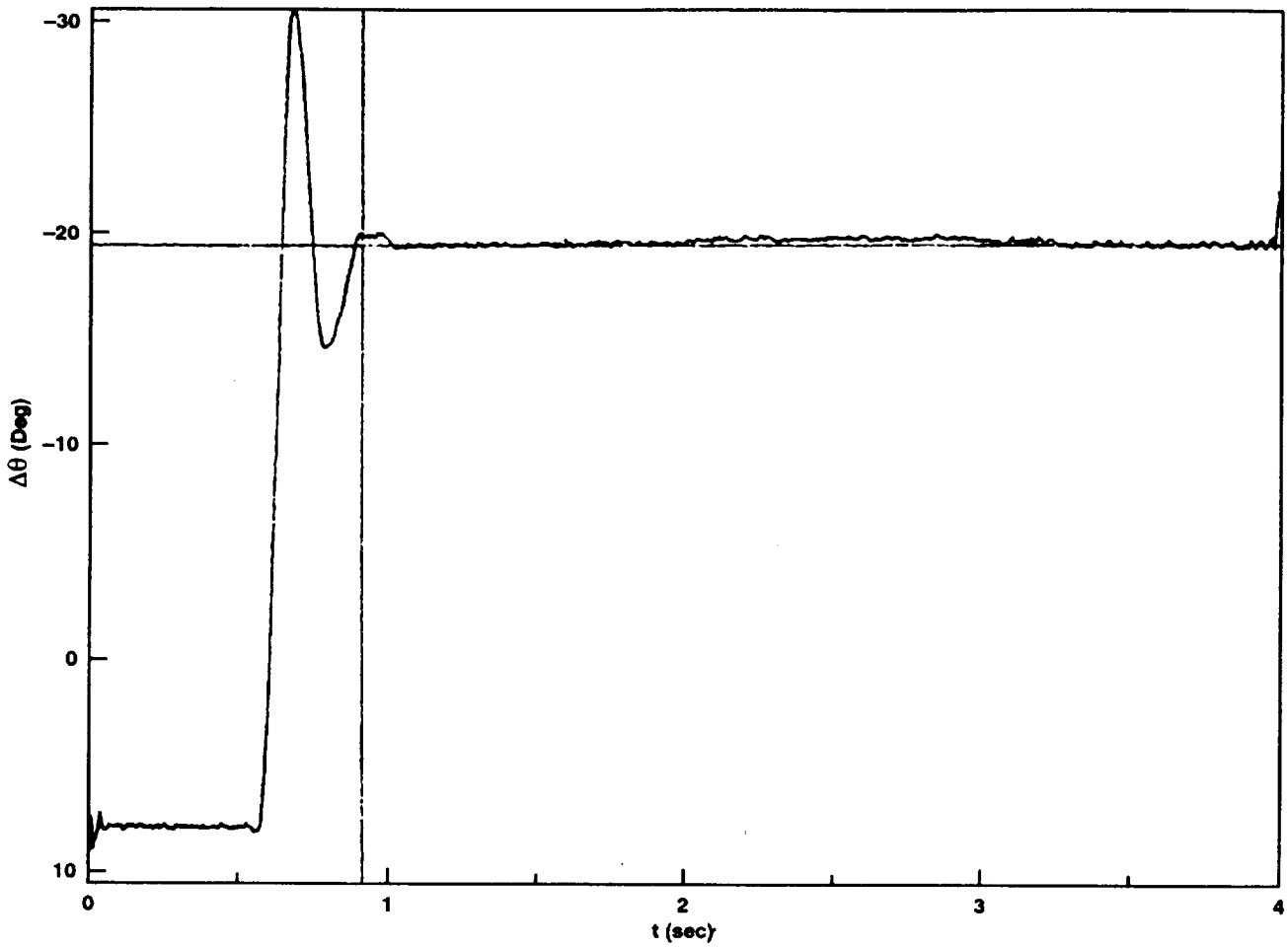

Fig. 4 Representative time history (FT35T3 tip, q = 0.38 kPa, α_W = 12 deg, θ_{PT} = 0 deg).

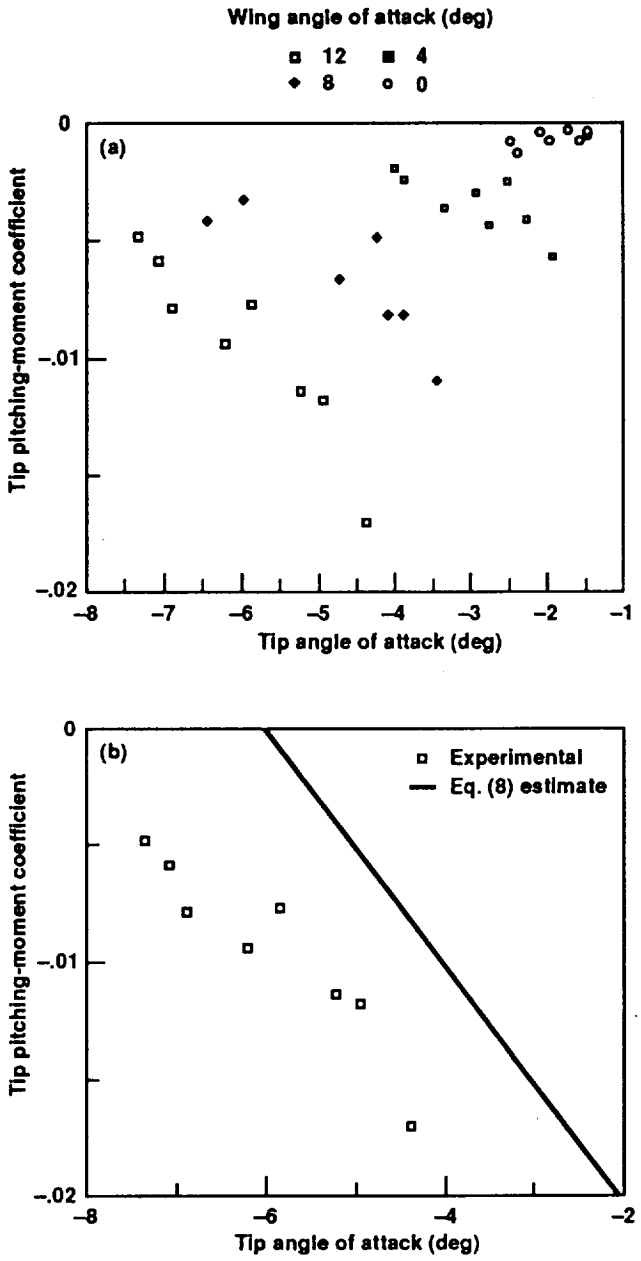

Fig. 5 Tip steady-state moment characteristics. a) Tip steady-state pitching-moment trend, b) validity of the semiempirical relationship in representing the tip-pitching-moment trend (wing angle of attack = 12 deg).

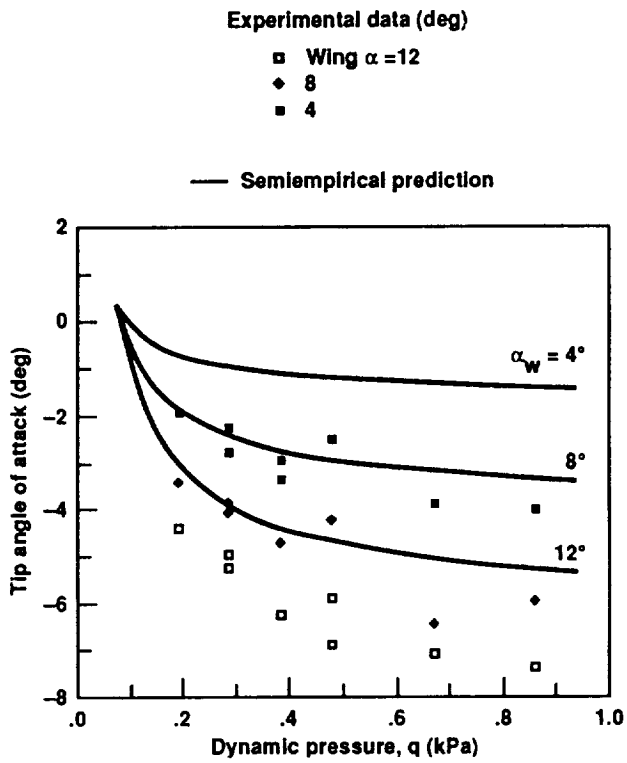

Fig. 6 Free-pitching tip steady-state angle of attack.

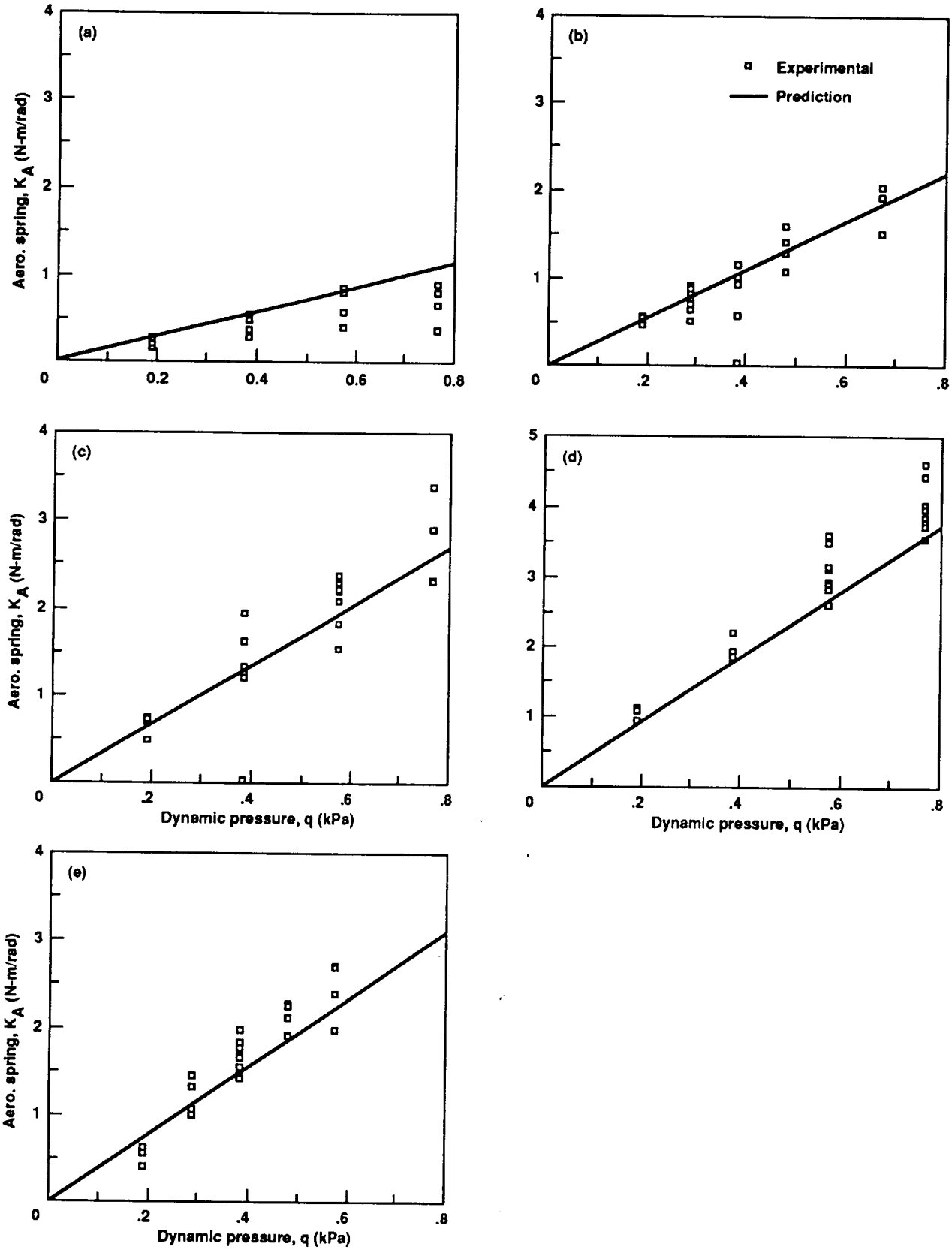

Fig. 7 Free-pitching tip aerodynamic spring trend. a) 20-deg swept tip with 0.3 taper, b) 35-deg swept tip with 0.3 taper, c) 35-deg swept tip with 0.6 taper, d) 45-deg swept tip with 0.6 taper, e) advanced configuration RC1008 tip.

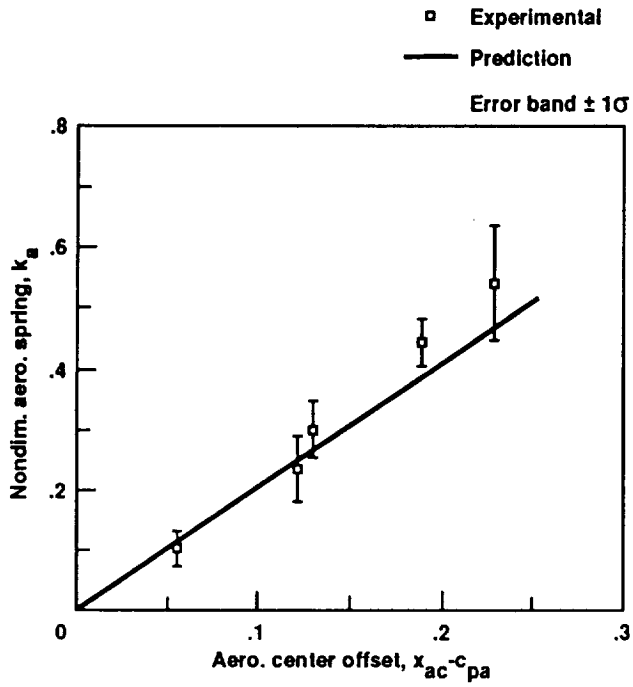

Fig. 8 Influence of tip aerodynamic center on aerodynamic spring.

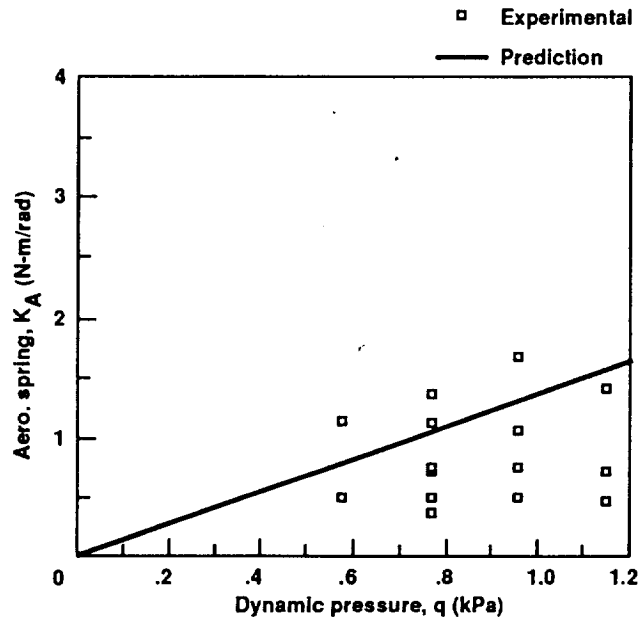

Fig. 9 Influence of wing sweep on tip aerodynamic spring (FT35T3 tip, 45-deg wing sweep).

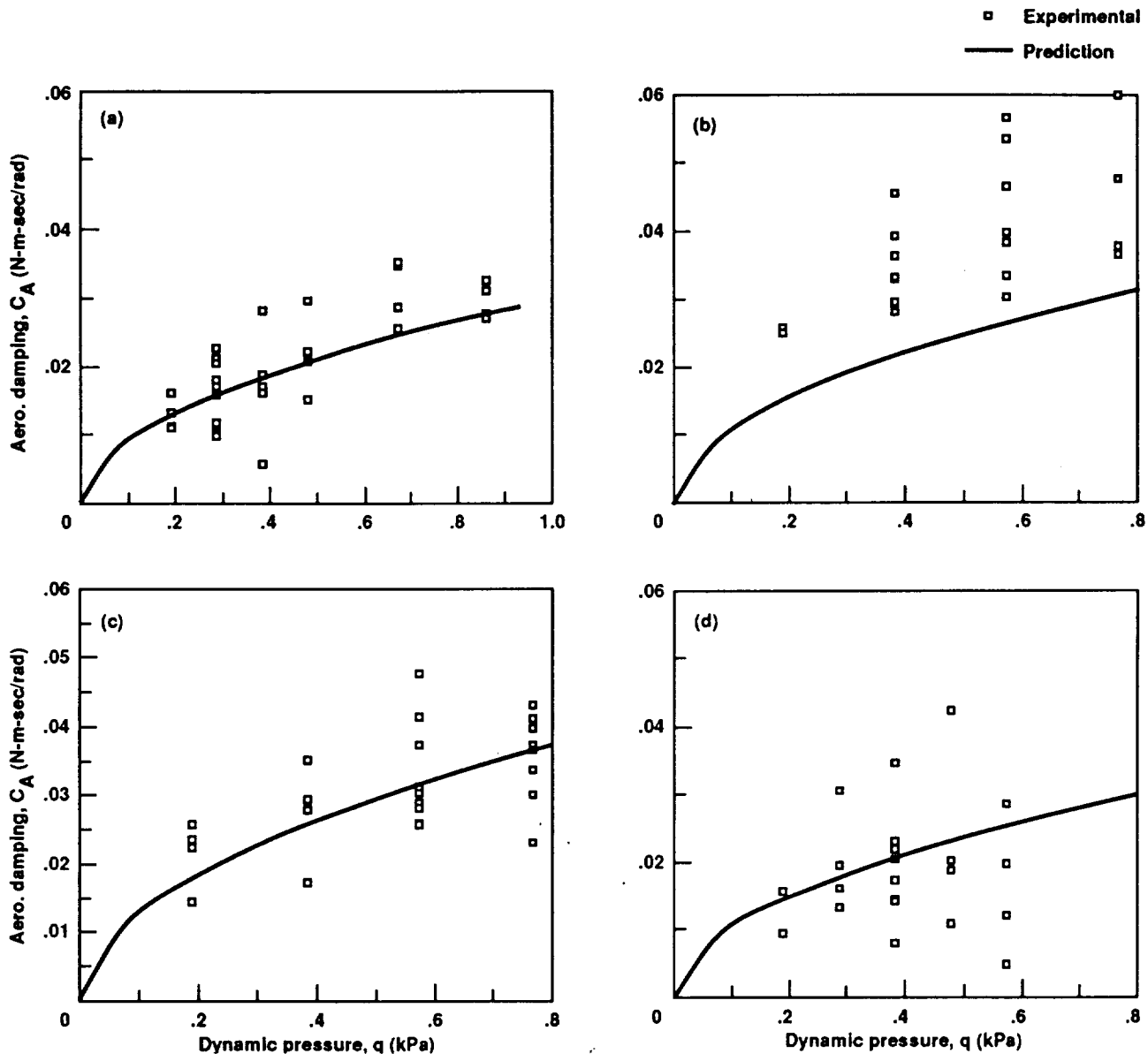

Fig. 10 Free-pitching tip aerodynamic damping trend. a) 35-deg swept tip with 0.3 taper, b) 35-deg swept tip with 0.6 taper, c) 45-deg swept tip with 0.6 taper, d) advanced configuration RC1008 tip.

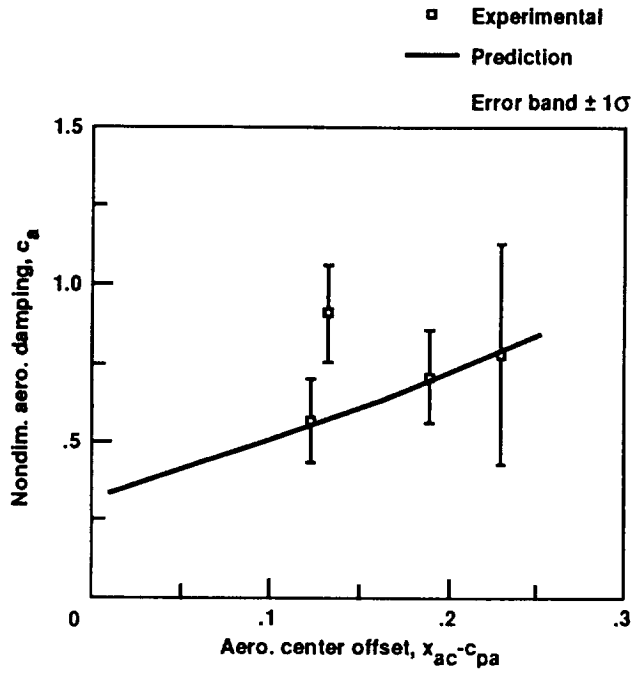

Fig. 11 Influence of tip aerodynamic center on aerodynamic damping.

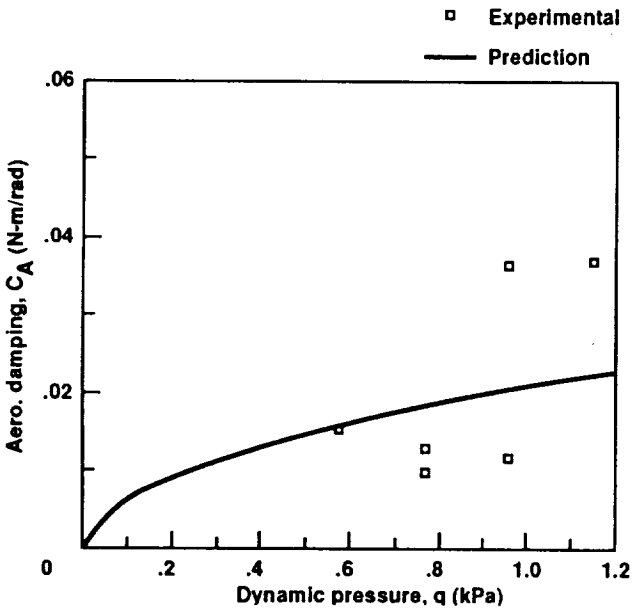

Fig. 12 Influence of wing sweep on tip aerodynamic damping (FT35T3 tip, 45-deg wing sweep).

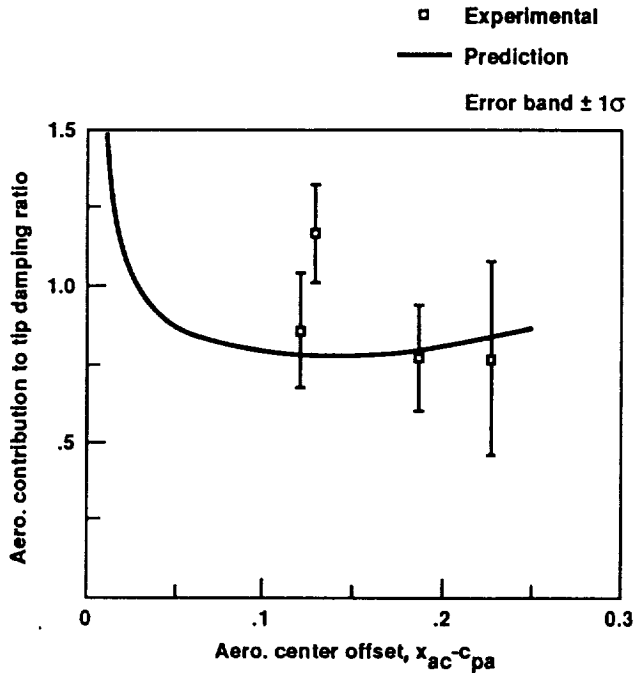

Fig. 13 Influence of tip planform on aerodynamic contribution of the tip damping ratio.